

Investigation of meson masses for real and imaginary chemical potential using the three-flavor PNJL model

Takeshi Matsumoto,^{1,*} Kouji Kashiwa,^{1,†} Hiroaki
Kouno,^{2,‡} Kagayaki Oda,^{1,§} and Masanobu Yahiro^{1,¶}

¹*Department of Physics, Graduate School of Sciences,
Kyushu University, Fukuoka 812-8581, Japan*

²*Department of Physics, Saga University, Saga 840-8502, Japan*

(Dated: February 4, 2022)

Abstract

We investigate chemical-potential (μ) and temperature (T) dependence of scalar and pseudo-scalar meson masses for both real and imaginary μ , using the Polyakov-loop extended Nambu–Jona-Lasinio (PNJL) model with three-flavor quarks. A three-flavor phase diagram is drawn in μ^2 - T plane where positive (negative) μ^2 corresponds to positive (imaginary) μ . A critical surface is plotted as a function of light- and strange-quark current mass and μ^2 . We show that μ -dependence of the six-quark Kobayashi-Maskawa–t Hooft (KMT) determinant interaction originated in $U_A(1)$ anomaly can be determined from lattice QCD data on η' meson mass around $\mu = 0$ and $\mu = i\pi T/3$ with T slightly above the critical temperature at $\mu = 0$ where the chiral symmetry is restored at $\mu = 0$ but broken at $\mu = i\pi T/3$, if it is measured in future.

PACS numbers: 11.30.Rd, 12.40.-y, 21.65.Qr, 25.75.Nq

*t-matsumoto@phys.kyushu-u.ac.jp

†kashiwa@phys.kyushu-u.ac.jp

‡kounoh@cc.saga-u.ac.jp

§oda@phys.kyushu-u.ac.jp

¶yahiro@phys.kyushu-u.ac.jp

I. INTRODUCTION

In recent theoretical studies, novel scenarios for QCD phase structure at finite real chemical potential (μ_R) are suggested; for example, the quarkyonic phase [1–4], the multi critical-endpoint generation [5–8] and the Lifshitz-point induced by the inhomogeneous phase [9]. Thus, *qualitative or speculative* investigation of QCD phase diagram is progressing well.

Nevertheless, *quantitative or more conclusive* understanding of QCD phase diagram is quite poor. The principal reason is the sign problem in the first-principle lattice QCD simulation at finite μ_R . Several methods such as the reweighting method [10], the Taylor expansion method [11], the analytic continuation from imaginary chemical potential μ_I to μ_R [12–14] and so on were proposed so far to circumvent the sign problem. However, they do not reach the $\mu_R/T \gtrsim 1$ region yet. For this reason, effective models such as the Nambu–Jona-Lasinio (NJL) model were used so far to investigate qualitative properties of the phase structure at finite μ_R . The effective-model approach, however, has an ambiguity particularly in the interaction part; see Ref. [15] and references therein.

Thus, a new approach should be proposed for quantitative or more reliable investigation of QCD phase diagram at finite μ_R . As a possible answer, recently, we proposed the *imaginary chemical potential matching approach* (the μ_I -matching approach) [16, 17]. In this approach, interactions of the effective model are determined from LQCD data at finite μ_I where no sign problem comes out. After the determination, a phase structure at finite μ_R is predicted with the effective model. The most important point in this approach is whether the model taken can reproduce the Roberge-Weiss (RW) periodicity and the RW transition at finite μ_I [18]. In our previous works [16], we showed that the Polyakov-loop extended Nambu–Jona-Lasinio (PNJL) model [19] can do it, because the thermodynamical potential of the PNJL model is invariant under the extended \mathbb{Z}_3 transformation of

$$e^{\pm i\theta} \rightarrow e^{\pm i\theta} e^{\pm i\frac{2\pi k}{3}}, \quad \Phi(\theta) \rightarrow \Phi(\theta) e^{-i\frac{2\pi k}{3}}, \quad \bar{\Phi}(\theta) \rightarrow \bar{\Phi}(\theta) e^{i\frac{2\pi k}{3}}, \quad (1)$$

where $\theta = \mu_I/T$. Here, Φ and $\bar{\Phi}$ denote the Polyakov-loop and its conjugate, respectively. This symmetry ensures the RW periodicity. Since, the PNJL model is designed to treat the confinement mechanism approximately in addition to the chiral symmetry breaking, we can investigate not only the chiral transition but also the deconfinement transition with the PNJL model. We also showed by using the PNJL model that the crossover deconfinement transition that takes place at finite θ becomes stronger as θ increases and eventually at $\theta = \pi/3$ it changes into the RW phase transition [16].

The $U_A(1)$ anomaly related to instantons can be taken into account in the NJL and PNJL models. In the three-flavor case, it is described by the effective six-quark Kobayashi-Maskawa-'t Hooft (KMT) determinant interaction [20, 21]. The $U_A(1)$ anomaly restoration at finite T in the case of $\mu = 0$ is investigated by the NJL model [22] that can reproduce the lattice QCD data [23]. At finite μ_R , μ -dependence of the anomaly restoration strongly depends on that of coupling constant G_D of the KMT determinant interaction [24]. However, μ -dependence of G_D is unclear, because lattice QCD data is not feasible at finite μ_R and also theoretical understanding on μ -dependence of the instanton density is not sufficient. Therefore, the phase structure in the three-flavor system is more ambiguous than in the two-flavor system.

In this paper, we investigate scalar and pseudo-scalar meson masses in both the μ_R and μ_I regions, using the three-flavor PNJL model. We show η' meson mass is sensitive to G_D particularly near $\theta = \pi/3$. This means that the θ dependence of η' meson mass is a good quantity to determine μ dependence of G_D . At the present stage, there is no reliable lattice QCD data particular on meson masses for the case of finite μ_I . Therefore, our investigation is limited to only a qualitative level.

II. THREE-FLAVOR PNJL MODEL

Lagrangian density of the three-flavor PNJL model is

$$\begin{aligned} \mathcal{L}_{\text{PNJL}} = & \bar{q}(i\gamma_\nu D^\nu - \hat{m}_0)q + G_S \sum_{a=0}^8 [(\bar{q}\lambda_a q)^2 + (\bar{q}i\gamma_5 \lambda_a q)^2] \\ & - G_D \left[\det_{ij} \bar{q}_i(1 + \gamma_5)q_j + \det_{ij} \bar{q}_i(1 - \gamma_5)q_j \right] - \mathcal{U}(\Phi[A], \bar{\Phi}[A], T), \end{aligned} \quad (2)$$

where $D^\nu = \partial^\nu + iA^\nu = \partial^\nu + i\delta_0^\nu g A_a^0 \lambda_a/2$ with the gauge coupling g and the Gell-Mann matrices λ_a . Three-flavor quark fields $q = (q_u, q_d, q_s)$ have current quark masses $\hat{m}_0 = \text{diag}(m_u, m_d, m_s)$. The Polyakov potential \mathcal{U} is defined later in (7) and (8). In the interaction part, G_S and G_D denote coupling constants of the scalar-type four-quark and the KMT determinant interaction, respectively. The determinant \det_{ij} runs in the flavor space and then the KMT determinant interaction breaks the $U_A(1)$ symmetry explicitly.

In the PNJL model, the gauge field A_μ is treated as a homogeneous and static background field. The Polyakov-loop Φ and its conjugate $\bar{\Phi}$ are given by

$$\Phi = \frac{1}{3}\text{tr}_c(L), \quad \bar{\Phi} = \frac{1}{3}\text{tr}_c(\bar{L}) \quad (3)$$

where $L = \exp(iA_4/T)$ with $A_4 = iA_0$ in Euclidean space. In the Polyakov-gauge, A_4 is diagonal in the color space.

We make the mean field approximation (MFA) to the quark-quark interactions in (2) in the following way. In (2), the operator product $\bar{q}_i q_j$ is first divided into $\bar{q}_i q_j = \sigma_{ij} + (\bar{q}_i q_j)'$ with the mean field $\sigma_{ij} \equiv \langle \bar{q}_i q_j \rangle$ and the fluctuation $(\bar{q}_i q_j)'$ where $i, j = u, d, s$. Ignoring higher-order terms of $(\bar{q}_i q_j)'$ in the rewritten Lagrangian and re-substituting $(\bar{q}_i q_j)' = \bar{q}_i q_j - \sigma_{ij}$ into the approximated Lagrangian, one can obtain a linearized Lagrangian based on MFA:

$$\begin{aligned} \mathcal{L}_{\text{PNJL}}^{\text{MFA}} = & \bar{q}_i (i\gamma_\nu \partial^\nu + i\gamma_0 A_4 - M_{ii}) q_i - \left(\sum_{i=u,d,s} 2G_S \sigma_{ii}^2 - 4G_D \sigma_{uu} \sigma_{dd} \sigma_{ss} \right) \\ & - \mathcal{U}(\Phi[A], \bar{\Phi}[A], T), \end{aligned} \quad (4)$$

where the dynamical quark mass M_{ii} is defined by $M_{ii} = m_i - 4G_S \sigma_{ii} + 2G_D \sigma_{jj} \sigma_{kk}$ with $i \neq j \neq k$.

In this study, we impose the isospin symmetry for u - d sector and then we use $m_l = m_u = m_d$. The thermodynamical potential becomes

$$\begin{aligned} \Omega_{\text{PNJL}} = & -2 \sum_{f=u,d,s} \int \frac{d^3 p}{(2\pi)^3} \left[N_c E_{p,f} \right. \\ & + \frac{1}{\beta} \ln [1 + 3(\Phi + \bar{\Phi} e^{-\beta(E_{p,f} - \mu_f)}) e^{-\beta(E_{p,f} - \mu_f)} + e^{-3\beta(E_{p,f} - \mu_f)}] \\ & + \frac{1}{\beta} \ln [1 + 3(\bar{\Phi} + \Phi e^{-\beta(E_{p,f} + \mu_f)}) e^{-\beta(E_{p,f} + \mu_f)} + e^{-3\beta(E_{p,f} + \mu_f)}] \Big] \\ & + \left(\sum_{i=u,d,s} 2G_S \sigma_{ii}^2 - 4G_D \sigma_{uu} \sigma_{dd} \sigma_{ss} \right) + \mathcal{U}(\Phi[A], \bar{\Phi}[A], T). \end{aligned} \quad (5)$$

We take the three-dimensional momentum cutoff,

$$\int \frac{d^3 p}{(2\pi)^3} \rightarrow \frac{1}{2\pi^2} \int_0^\Lambda dp p^2, \quad (6)$$

because this model is non-renormalizable. Hence, the present model has five parameters G_S , G_D , m_l , m_s and Λ . We use the parameter set determined in Ref. [25]; these are fitted to the empirical values of π meson mass and its decay constant, K meson mass and its decay constant and η' meson mass. We also use \mathcal{U} of Ref. [26] fitted to LQCD data in the pure gauge limit at finite T [27, 28]:

$$\frac{\mathcal{U}}{T^4} = -\frac{b_2(T)}{2} \bar{\Phi} \Phi - \frac{b_3}{6} (\bar{\Phi}^3 + \Phi^3) + \frac{b_4}{4} (\bar{\Phi} \Phi)^2, \quad (7)$$

$$b_2(T) = a_0 + a_1 \left(\frac{T_0}{T} \right) + a_2 \left(\frac{T_0}{T} \right)^2 + a_3 \left(\frac{T_0}{T} \right)^3. \quad (8)$$

In this study, we take the original value $T_0 = 270$ MeV.

III. MESON MASS FORMALISM

First, Lagrangian density (4) is rewritten by MFA into

$$\begin{aligned} \mathcal{L} = & \bar{q}_i(i\gamma_\nu D^\nu - \hat{m}_0)q_j + \sum_{a=0}^8 [G_a^-(\bar{q}\lambda_a q)^2 + G_a^+(\bar{q}i\gamma_5\lambda_a q)^2] \\ & + \sum_{a,b=0,3,8} [G_{ab}^-(\bar{q}\lambda_a q)(\bar{q}\lambda_b q) + G_{ab}^+(\bar{q}i\gamma_5\lambda_a q)(\bar{q}i\gamma_5\lambda_b q)] \end{aligned} \quad (9)$$

with

$$\left\{ \begin{array}{ll} G_0^\pm = G_S \mp \frac{1}{3}G_D(\sigma_{uu} + \sigma_{dd} + \sigma_{ss}), & G_1^\pm = G_2^\pm = G_3^\pm = G_S \pm \frac{1}{2}G_D\sigma_{ss}, \\ G_4^\pm = G_5^\pm = G_S \pm \frac{1}{2}G_D\sigma_{dd}, & G_6^\pm = G_7^\pm = G_S \pm \frac{1}{2}G_D\sigma_{uu}, \\ G_8^\pm = G_S \pm \frac{1}{6}G_D(2\sigma_{uu} + 2\sigma_{dd} - \sigma_{ss}), & G_{30}^\pm = G_{03}^\pm = \mp \frac{1}{2\sqrt{6}}G_D(\sigma_{uu} - \sigma_{dd}), \\ G_{08}^\pm = G_{80}^\pm = \pm \frac{\sqrt{2}}{12}G_D(\sigma_{uu} + \sigma_{dd} - 2\sigma_{ss}), & G_{38}^\pm = G_{83}^\pm = \pm \frac{1}{2\sqrt{3}}G_D(\sigma_{uu} - \sigma_{dd}). \end{array} \right. \quad (10)$$

In the present case that the isospin symmetry is imposed in the u - d sector, we have $G_{30}^\pm = G_{03}^\pm = G_{38}^\pm = G_{83}^\pm = 0$.

Taking the same procedure as in the two-flavor case [17], we can obtain dynamical meson masses from poles of the effective propagator [25]:

$$\frac{2iG_i}{1 - 2G_i\Pi(q_0)} \rightarrow \left(1 - 2G_i\Pi(q_0)\right)\Big|_{q_0=M_\xi} = 0 \quad (11)$$

where Π denotes the Polarization function. The subscript i stands for meson ξ in a state i . The polarization function between states i and j is represented by

$$\Pi_{ij}(q) = -i \int \frac{d^4p}{(2\pi)^4} \text{Tr} \left[\Gamma(T_i) S_F(p) \Gamma(T_j) S_F(p - q) \right], \quad (12)$$

where S_F denotes the quark propagator and the vertex function Γ is **1** for the scalar meson and $i\gamma_5$ for the pseudo-scalar meson. The matrices T_i in flavor space depend on meson considered; for example, $T_i = T_j = \lambda_3$ for π and a_0 mesons and $T_i = (\lambda_6 + i\lambda_7)/\sqrt{2}$, $T_j = (\lambda_6 + i\lambda_7)/\sqrt{2}$ for K and κ mesons. When T and μ are finite, the corresponding equations are obtained by the replacement

$$\begin{aligned} p_0 & \rightarrow i\omega_n + \mu - iA_4 = i\pi T(2n + 1) + \mu - iA_4, \\ \int \frac{d^4p}{(2\pi)^4} & \rightarrow iT \sum_n \int \frac{d^3p}{(2\pi)^3}. \end{aligned} \quad (13)$$

As for η and η' mesons, the effective coupling constant G^\pm and the polarization function Π are 2×2 matrices in flavor space, since the isospin symmetry is imposed for the u - d sector:

$$G^\pm = \begin{bmatrix} G_{00}^\pm & G_{08}^\pm \\ G_{80}^\pm & G_{88}^\pm \end{bmatrix}, \quad \Pi = \begin{bmatrix} \Pi_{00} & \Pi_{08} \\ \Pi_{80} & \Pi_{88} \end{bmatrix}, \quad (14)$$

where

$$\Pi_{00} = \frac{1}{3} [2\Pi^{ll} + \Pi^{ss}], \quad \Pi_{88} = \frac{1}{3} [\Pi^{ll} + 2\Pi^{ss}], \quad \Pi_{08} = \Pi_{80} = \frac{\sqrt{2}}{6} [\Pi^{ll} - \Pi^{ss}]. \quad (15)$$

Here, the polarization function Π^{ff} for each flavor f is defined by

$$\Pi^{ff}(q) = -2i \int \frac{d^4 p}{(2\pi)^4} \text{Tr}_{C,D} [\Gamma S_F^f(p) \Gamma S_F^f(p-q)] \quad (16)$$

with $S_F^f(q)$ the propagator of quark with flavor f , where in $\text{Tr}_{C,D}$ the trace is taken for color and Dirac indices. Therefore, η and η' meson masses satisfy

$$\det(1 - 2G^+ \Pi) = 0. \quad (17)$$

This equation has two solutions; the lower corresponds to η meson mass, while the higher does to η' meson mass. Masses of σ and f_0 meson are obtained by replacing G^+ by G^- in (17) and setting $\Gamma = 1$ in (16).

IV. NUMERICAL RESULTS

Figure 1 shows the phase diagram in $\mu^2 - T$ plane for the three-flavor case. The positive (negative) μ^2 half-plane means real (imaginary) μ . In the present parameter set, a critical endpoint arises in the positive μ^2 half-plane, while a RW endpoint does at $\mu^2 = -(\pi T/3)^2$ with $T \approx 250$ MeV in the negative μ^2 half-plane. At the RW endpoint, the phase transition is second order. In the two-flavor case, as shown in [29], the order of RW phase transition at RW endpoint depends on the Polyakov potential \mathcal{U} taken; it is second order for \mathcal{U} of Ref. [19], but first order for \mathcal{U} of Ref. [30]. And the latter gives a result more consistent with lattice QCD data at finite μ_I than the former. This sort of analysis is quite important also for the three-flavor case in order to determine the form of \mathcal{U} , if precise lattice QCD data on the RW endpoint become available in future.

The critical endpoint (closed circle) in Fig. 1 is a function of m_l , m_s and μ^2 . This is described as a surface in the m_l - m_s - μ^2 space. The surface, usually called the critical surface, is plotted

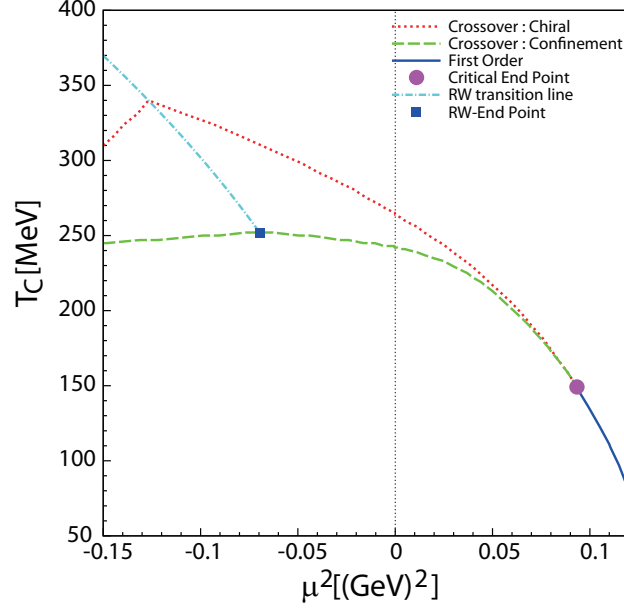


Fig. 1: (Color online) Phase diagram in $\mu^2 - T$ plane for the three-flavor case. The solid (dotted) line denotes a first-order (crossover) chiral transition, while the dot-dashed (dashed) line does a first-order RW (crossover deconfinement) transition. The closed circle (square) stands for an endpoint of the first-order chiral (RW) phase transition.

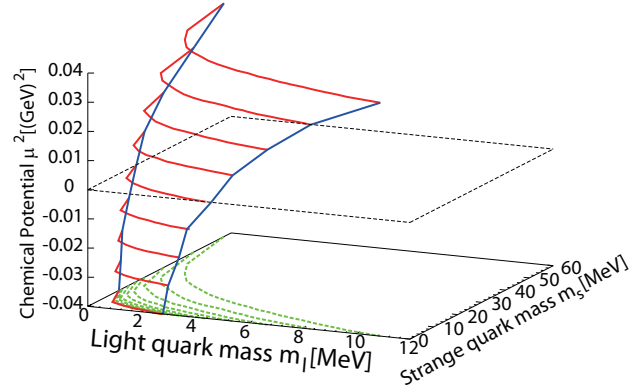


Fig. 2: (Color online) Critical surface as a function of m_l , m_s and μ^2 in the μ_R and μ_I regions.

in Fig. 2. In the present model, the critical surface has a positive curvature and then a critical endpoint arises somewhere in the $\mu^2 - T$ plane, as shown in Fig. 1, when m_l and m_s are taken to be physical values. This result may change, if the coupling constant G_D of KMT determinant interaction depends on μ [24]. However, the μ -dependent G_D of Ref. [24] can not be applicable to

the imaginary μ region, since it breaks the extended \mathbb{Z}_3 symmetry, i.e. the RW periodicity. Thus, at the present stage, we have no way of determining μ dependence of G_D . We then do not consider any μ -dependent G_D in this paper.

In Fig. 3, we investigate μ^2 -dependence of meson mass for mesons (π , K , η , η' , σ , κ , a_0 , f_0), using the PNJL model in which G_D is a constant $G_D = G_D(0) = -12.36\Lambda^{-5}$ where $G_D(0)$ is determined at $T = \mu = 0$. The left and the right panels correspond to $T = 200$ and 300 MeV, respectively. Furthermore, Figure 4 shows θ dependence of meson mass for $T = 300$ MeV; the left (right) panel corresponds to π and σ (K and κ). Obviously, these meson masses are θ -even and have the RW periodicity. Pion mass has dips at $\mu^2 \approx 0.06$ (GeV)² in panel (b), at $\mu^2 \approx -0.08$ (GeV)² in panel (d) of Fig. 3 and at $\theta \approx \pm 0.7$ and ± 1.3 MeV of Fig. 4. These are threshold effects due to $\pi \rightarrow \text{quark} + \text{antiquark}$.

A mass difference between the chiral partners π and σ is a good indicator of the chiral symmetry; the symmetry is restored (broken) when the difference is small (large). As for $T = 300$ MeV, as shown in panel (c) of Fig. 3 and the left panel of Fig. 4, the chiral symmetry is restored at $\mu^2 \gtrsim -0.02$ (GeV)², but broken at $\mu^2 \lesssim -0.02$ (GeV)² ($\pi/6 \lesssim \theta \leq \pi/3$). As for $T = 200$ MeV, as shown in panel (a) of Fig. 3, the symmetry is restored at $\mu^2 \gtrsim 0.1$ (GeV)², but broken at $\mu^2 \lesssim 0.1$ (GeV)². As an interesting result in Fig. 3, panels (c) and (d) almost agree with panels (a) and (b), respectively, if in panels (c) and (d) the μ^2 scale is shifted to the left by about 0.1. Thus, shifting the μ^2 scale to the left corresponds to looking at meson mass at lower T . If meson mass is measured in future by lattice QCD in the negative μ^2 region for some temperature T_{Latt} , the behavior qualitatively agrees with that in the positive μ^2 region for temperature lower than T_{Latt} . Therefore, we can predict qualitative behavior of meson mass in the positive μ^2 region from lattice data on meson mass in the negative μ^2 region.

Next, it is investigated how the KMT determinant interaction affects meson mass at imaginary μ by changing the value of G_D from the original one $G_D(0)$. As mentioned above, theoretically, G_D is allowed to have μ dependence. However, since the actual form is unknown, we simply change the value of G_D in the present analysis. Figure 5 shows π and σ meson masses at $T = 300$ MeV with the KMT determinant interaction in which $G_D = 0$ for left panel and $G_D = G_D(0)/2$ for right panel. As G_D increases, the π meson mass is reduced with almost keeping the θ dependence. The σ meson mass is also reduced, but the θ dependence is changed a lot around $\theta = \pi/3$. The left (right) panel of Fig. 6 shows η (η') meson mass at $T = 300$ MeV in three cases of $G_D = 0$, $G_D(0)/2$ and $G_D(0)$. The η meson mass has a similar property to the σ meson mass. Most

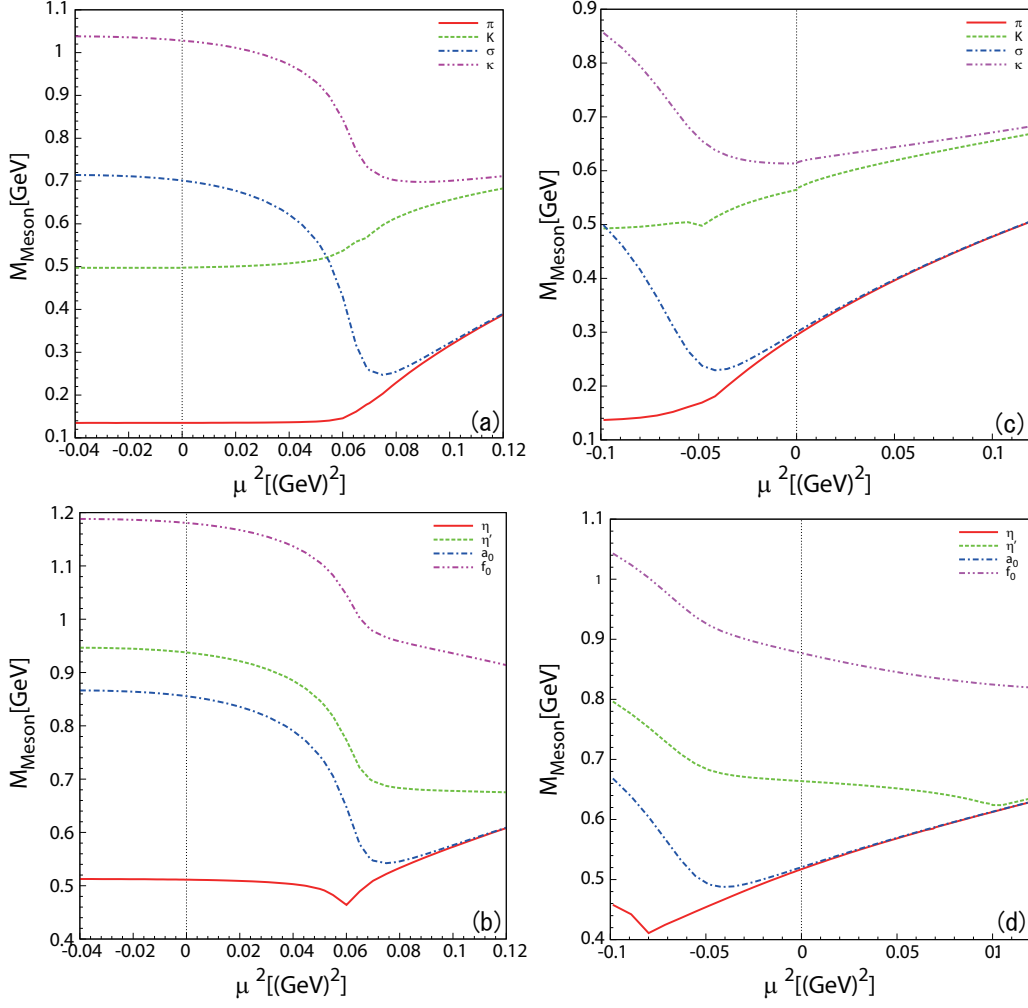


Fig. 3: (Color online) μ^2 -dependence of meson mass for (a) π , σ , K and κ at $T = 200$ MeV, (b) η , η' , a_0 and f_0 at $T = 200$ MeV, (c) π , σ , K and κ at $T = 300$ MeV, and (d) η , η' , a_0 and f_0 at $T = 300$ MeV.

interesting and important property is θ dependence of η' meson mass. The η' meson mass has a weak G_D dependence at $\theta = 0$, but the G_D dependence becomes strong around $\theta = \pi/3$. Thus, θ dependence of G_D that is allowed theoretically can be determined from that of η' meson mass, if it is measured in future by lattice QCD.

The sensitivity of η' meson mass to G_D around $\theta = \pi/3$ can be understood in the following. The KMT determinant interaction affects the meson mass only through the dynamical quark mass $M_{ii} = m_i - 4G_S\sigma_{ii} + 2G_D\sigma_{jj}\sigma_{kk}$ with a G_D dependent term of form $G_D\sigma_{ii}\sigma_{jj}$. The term $G_D\sigma_{ii}\sigma_{jj}$ is strongly suppressed when the chiral symmetry is restored, even if G_D is large. Hence, the $U_A(1)$ anomaly affects the meson mass only when the chiral symmetry is broken. As shown in Fig. 1, the

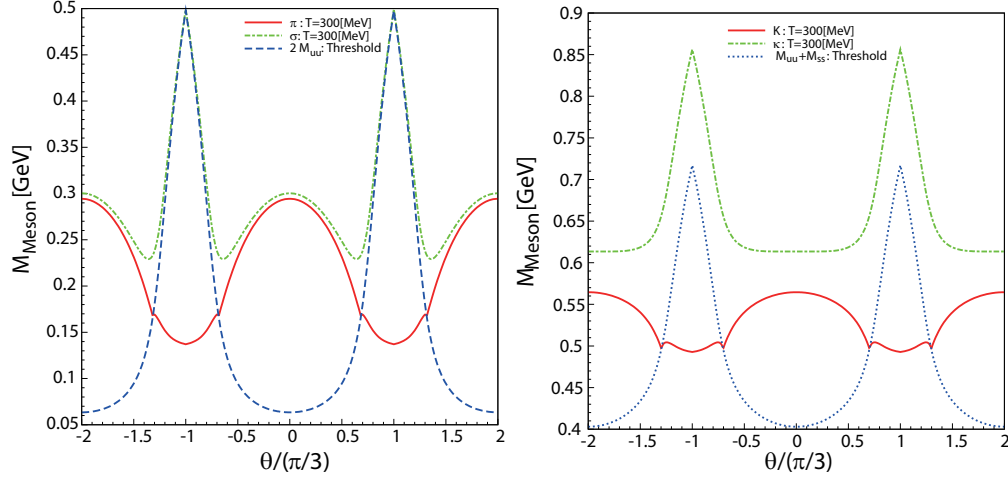


Fig. 4: (Color online) Meson mass at $T = 300$ MeV as a function of $\theta/(\pi/3)$. The left panel corresponds to π and σ , while the right panel does to K and κ .

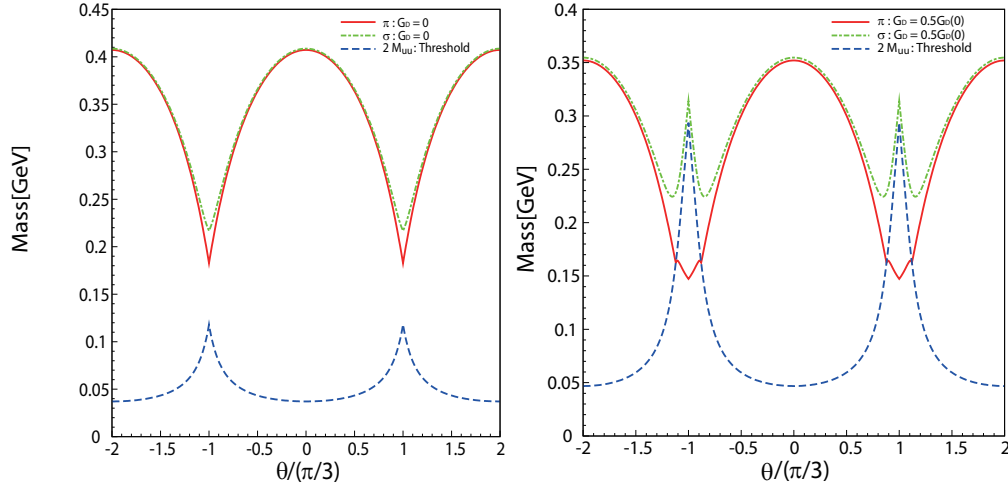


Fig. 5: (Color online) θ -dependence of σ and π meson masses at $T = 300$ MeV for $G_D = 0$ in the left panel and for $G_D = G_D(0)/2$ in the right panel.

critical temperature of the chiral transition goes up as θ increases from 0 to $\pi/3$. Thus, η' meson mass is most sensitive to G_D at $\theta = \pi/3$ when θ increases from 0 to $\pi/3$ with temperature fixed, because σ_{ii} and σ_{jj} are largest there.

In this study, G_D is assumed to be constant. If η' meson mass is measured by three-flavor lattice QCD in future, there is a possibility that the PNJL model with constant G_D can not reproduce lattice QCD data. If so, the deviation can determine θ -dependence of G_D and hence μ_R -dependence

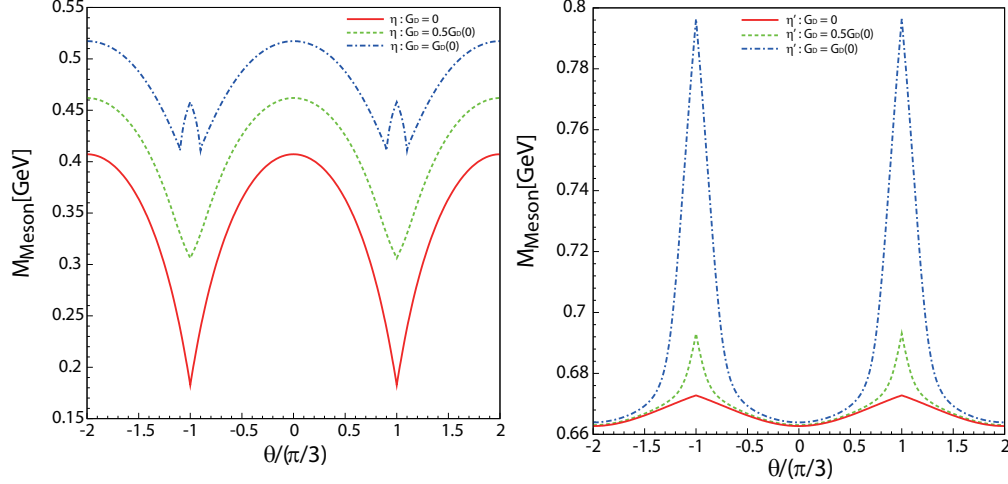


Fig. 6: (Color online) θ -dependence of meson mass at $T = 300$ MeV for η in left panel and η' in right panel. Three values of $G_D = 0$, $G_D(0)/2$ and $G_D(0)$ are taken.

of G_D .

V. SUMMARY

Using the three-flavor PNJL model, we have analyzed μ -dependence of scalar and pseudo-scalar meson masses in both the real and the imaginary μ region. In the imaginary μ region, the meson masses are even functions of θ with the RW periodicity. As an interesting result, μ^2 dependence of meson mass in the negative μ^2 region at some temperature is close to that in the positive μ^2 region at temperatures lower than the temperature. If meson mass is measured in future by lattice QCD in the negative μ^2 region for some temperature T_{Latt} , the behavior qualitatively agrees with that in the positive μ^2 region for temperatures lower than T_{Latt} . Therefore, we can predict qualitative behavior of meson mass in the positive μ^2 region from lattice data on meson mass in the negative μ^2 region.

The $U_A(1)$ anomaly (the KMT determinant interaction) affects meson masses through the term $G_D \sigma_{jj} \sigma_{kk}$ in the dynamical quark mass M_{ii} . Particularly, the effect is remarkable for η' meson. For temperatures slightly above the critical temperature at $\theta = 0$, the chiral condensate increases a lot as θ increases from 0 to $\pi/3$, so that the effect has a strong θ dependence. We then recommend that meson masses, particularly η' meson mass, be measured by lattice QCD for $\theta = 0$ and $\pi/3$ at such higher temperatures. Using the lattice QCD data, we can determine T and μ dependences of

coupling constant G_D of the KMT determinant interaction and hence can predict the three-flavor phase diagram with higher reliability by the PNJL model.

Acknowledgments

The authors thank Dr. H. Kohyama for useful discussion. K.K. is supported by the Japan Society for the Promotion of Science for Young Scientists.

-
- [1] L. McLerran, and R. D. Pisarski, Nucl. Phys. **A796**, 83 (2007).
 - [2] Y. Hidaka, L. McLerran, and R. D. Pisarski, Nucl. Phys. **A808**, 117 (2008).
 - [3] L. McLerran, R. D. Pisarski, and C. Sasaki, arXiv:0812.3585 (2008).
 - [4] K. Miura, T. Z. Nakano, and A. Ohnishi, Prog. Theor. Phys. **122**, 1045 (2009).
 - [5] M. Kitazawa, T. Koide, T. Kunihiro, and Y. Nemoto, Prog. Theor. Phys. **108**, 929 (2002).
 - [6] T. Hatsuda, M. Tachibana, N. Yamamoto, and G. Baym, Phys. Rev. Lett. **97**, 122001 (2006).
 - [7] Z. Zhang, K. Fukushima, and T. Kunihiro, Phys. Rev. D **79**, 014004 (2009).
 - [8] M. Harada, C. Sasaki, and S. Takemoto, Phys. Rev. D **81**, 016009 (2010).
 - [9] D. Nickel, Phys. Rev. Lett. **103**, 072301 (2009); Phys. Rev. D **80**, 074025 (2009).
 - [10] Z. Fodor, and S. D. Katz, Phys. Lett. B **534**, 87 (2002); J. High Energy Phys. **03**, 014 (2002).
 - [11] C. R. Allton, S. Ejiri, S. J. Hands, O. Kaczmarek, F. Karsch, E. Laermann, Ch. Schmidt, and L. Scorzato, Phys. Rev. D **66**, 074507 (2002); S. Ejiri, C. R. Allton, S. J. Hands, O. Kaczmarek, F. Karsch, E. Laermann, and Ch. Schmidt, Prog. Theor. Phys. Suppl. **153**, 118 (2004).
 - [12] P. de Forcrand and O. Philipsen, Nucl. Phys. **B642**, 290 (2002); P. de Forcrand and O. Philipsen, Nucl. Phys. **B673**, 170 (2003).
 - [13] M. D'Elia and M. P. Lombardo, Phys. Rev. D **70**, 074509 (2004).
 - [14] M. D'Elia and M. P. Lombardo, Phys. Rev. D **67**, 014505 (2003); M. P. Lombardo, PoSCPOD2006, 003 (2006).
 - [15] K. Kashiwa, H. Kouno, M. Matsuzaki, and M. Yahiro, Phys. Lett. B **662**, 26 (2008).
 - [16] Y. Sakai, K. Kashiwa, H. Kouno, and M. Yahiro, Phys. Rev. D **77**, 051901(R) (2008); Phys. Rev. D **78**, 036001 (2008); Y. Sakai, K. Kashiwa, H. Kouno, M. Matsuzaki, and M. Yahiro, Phys. Rev. D **78**, 076007 (2008); Phys. Rev. D **79**, 096001 (2009); K. Kashiwa, M. Yahiro, H. Kouno, M. Matsuzaki,

- and Y. Sakai, J. Phys. G: Nucl. Part. Phys. **36**, 105001 (2009). H. Kouno, Y. Sakai, K. Kashiwa, and M. Yahiro, J. Phys. G: Nucl. Part. Phys. **36**, 115010 (2009);
- [17] K. Kashiwa, M. Matsuzaki, H. Kouno, Y. Sakai, and M. Yahiro, Phys. Rev. D **79**, 076008 (2009).
- [18] A. Roberge and N. Weiss, Nucl. Phys. **B275**, 734 (1986).
- [19] K. Fukushima, Phys. Lett. B **591**, 277 (2004); Phys. Rev. D **77**, 114028 (2008); Phys. Rev. D **78**, 114019 (2008).
- [20] M. Kobayashi, and T. Maskawa, Prog. Theor. Phys. **44**, 1422 (1970); M. Kobayashi, H. Kondo, and T. Maskawa, Prog. Theor. Phys. **45**, 1955 (1971).
- [21] G. 't Hooft, Phys. Rev. Lett. **37**, 8 (1976); Phys. Rev. D **14**, 3432 (1976); **18**, 2199(E) (1978).
- [22] K. Fukushima, K. Ohnishi, and K. Ohta, Phys. Rev. C **63**, 045203 (2001); Phys. Lett. B **514**, 200 (2001).
- [23] B. Allés, M. D'Elia, and A. Di Giacomo, Nucl. Phys. **B494**, 281 (1997); **B679**, 397(E) (2004).
- [24] J.-W. Chen, K. Fukushima, H. Kohyama, K. Ohnishi, and U. Raha, Phys. Rev. D **80**, 054012 (2009).
- [25] S. P. Klevansky, Rev. Mod. Phys. **64**, 649 (1992).
- [26] C. Ratti, M. A. Thaler, and W. Weise, Phys. Rev. D **73**, 014019 (2006).
- [27] G. Boyd, J. Engels, F. Karsch, E. Laermann, C. Legeland, M. Lütgemeier, and B. Petersson, Nucl. Phys. **B469**, 419 (1996).
- [28] O. Kaczmarek, F. Karsch, P. Petreczky, and F. Zantow, Phys. Lett. B **543**, 41 (2002).
- [29] Y. Sakai, H. Kouno and M. Yahiro, arXiv:0908.3088 [hep-ph].
- [30] S. Rößner, C. Ratti, and W. Weise, Phys. Rev. D **75**, 034007 (2007).